

Realization of arbitrary two-qubit quantum gates based on chiral Majorana fermions

Qing Yan(闫青) and Qing-Feng Sun(孙庆丰)

Citation: Chin. Phys. B, 2021, 30 (**4**): 040303. DOI: 10.1088/1674-1056/abe296
Journal homepage: http://cpb.iphy.ac.cn; http://iopscience.iop.org/cpb

What follows is a list of articles you may be interested in

Efficient self-testing system for quantum computations based on permutations

Shuquan Ma(马树泉), Changhua Zhu(朱畅华), Min Nie(聂敏), and Dongxiao Quan(权东晓)
Chin. Phys. B, 2021, 30 (**4**): 040305. DOI: 10.1088/1674-1056/abe29a

Taking tomographic measurements for photonic qubits 88 ns before they are created

Zhibo Hou(侯志博), Qi Yin(殷琪), Chao Zhang(张超), Han-Sen Zhong(钟翰森), Guo-Yong Xiang(项国勇)†, Chuan-Feng Li(李传锋), Guang-Can Guo(郭光灿), Geoff J. Pryde, and Anthony Laing‡
Chin. Phys. B, 2021, 30 (**4**): 040304. DOI: 10.1088/1674-1056/abe29c

Nonlocal advantage of quantum coherence in a dephasing channel with memory

Ming-Liang Hu(胡明亮), Yu-Han Zhang(张宇晗), and Heng Fan(范桁)
Chin. Phys. B, 2021, 30 (**3**): 030308. DOI: 10.1088/1674-1056/abcf4a

A proposal for preparation of cluster states with linear optics

Le Ju(鞠乐), Ming Yang(杨名), and Peng Xue(薛鹏)
Chin. Phys. B, 2021, 30 (**3**): 030306. DOI: 10.1088/1674-1056/abd74b

Quantum algorithm for a set of quantum 2SAT problems

Yanglin Hu(胡杨林), Zhelun Zhang(张哲伦), and Biao Wu(吴飙)
Chin. Phys. B, 2021, 30 (**2**): 020308. DOI: 10.1088/1674-1056/abd741

SPECIAL TOPIC — Quantum computation and quantum simulation

Realization of arbitrary two-qubit quantum gates based on chiral Majorana fermions*

Qing Yan(闫青)[1,2] and Qing-Feng Sun(孙庆丰)[1,3,4,†]

[1] International Center for Quantum Materials, School of Physics, Peking University, Beijing 100871, China
[2] CAS Center for Excellence in Topological Quantum Computation, University of Chinese Academy of Sciences, Beijing 100190, China
[3] Collaborative Innovation Center of Quantum Matter, Beijing 100871, China
[4] Beijing Academy of Quantum Information Sciences, Beijing 100193, China

(Received 14 October 2020; revised manuscript received 26 December 2020; accepted manuscript online 3 February 2021)

Quantum computers are in hot-spot with the potential to handle more complex problems than classical computers can. Realizing the quantum computation requires the universal quantum gate set {T, H, CNOT} so as to perform any unitary transformation with arbitrary accuracy. Here we first briefly review the Majorana fermions and then propose the realization of arbitrary two-qubit quantum gates based on chiral Majorana fermions. Elementary cells consist of a quantum anomalous Hall insulator surrounded by a topological superconductor with electric gates and quantum-dot structures, which enable the braiding operation and the partial exchange operation. After defining a qubit by four chiral Majorana fermions, the single-qubit T and H quantum gates are realized via one partial exchange operation and three braiding operations, respectively. The entangled CNOT quantum gate is performed by braiding six chiral Majorana fermions. Besides, we design a powerful device with which arbitrary two-qubit quantum gates can be realized and take the quantum Fourier transform as an example to show that several quantum operations can be performed with this space-limited device. Thus, our proposal could inspire further utilization of mobile chiral Majorana edge states for faster quantum computation.

Keywords: quantum computation, T gate, CNOT gate, braiding, chiral Majorana fermions

PACS: 03.67.Lx, 74.78.−w, 73.21.La **DOI:** 10.1088/1674-1056/abe296

1. Introduction

Facing the dilemma caused by the increasing demand for data processing and the gradual failure of Moore's law, quantum computation arises to help to break this bottleneck, that is, to compute from the basic quantum-mechanic law rather than stimulate the quantum system in a classical way.[1,2] The power of quantum computation roots in the qubit: the information contained in one qubit, defined as the superposition of two basis states, is much more than that in one classical bit, just 0 and 1; the dimension of computational space grows exponentially as the number of qubits increases due to the exotic entanglement.[3] As one of the computational models, the quantum circuit model takes up the quantum gate to manipulate the qubit based on the original proposal by Benioff that a quantum computer would be constructed by the time evolution of a quantum system.[4] Similar to the XOR and AND gates in the classical computer, a finite set of quantum gates can accurately realize the arbitrary unitary transformation, i.e., the so-called universal quantum gate set {T, H, CNOT}.[5] The design and fabrication of qubits and quantum gates have brought quantum computing into a promising and challenging research field.

Along the way of pursuing a quantum computer, the first step is to fabricate the qubit in a physical system. Among various two-level systems, some with long coherent time have been proposed to serve as a qubit, including photons,[6] trapped atoms,[7,8] quantum dots,[9–11] superconducting Josephson junctions,[12–15] etc. Besides these conventional devices, recent interests in topology claim that a topological system owns a natural advantage of protection against local perturbations, thus opening up a research field called topological quantum computation.[16] The Majorana system, simple but nontrivial, is considered as a potential platform for fault-tolerant topological quantum computation.[17]

In condensed matter physics, Majorana fermions represent a kind of self-conjugate quasiparticle excitations, i.e., $\gamma^\dagger = \gamma$ in the operator language.[18] The reality of wave function requires the phase of a Majorana fermion to be either 0 or π. A Majorana fermion is usually regarded as a half of a Dirac fermion, since an ordinary electron and a hole can be reorganized and divided into two real Majorana fermions.[19] In turn, two Majorana fermions form a nonlocal ordinary fermion level with a well-defined occupation number, which is protected by the gap. Besides, Majorana zero modes (MZMs),

*Project supported by the National Key R&D Program of China (Grant No. 2017YFA0303301), the National Natural Science Foundation of China (Grant No. 11921005), the Strategic Priority Research Program of Chinese Academy of Sciences (Grant No. XDB28000000), and Beijing Municipal Science & Technology Commission, China (Grant No. Z191100007219013).

†Corresponding author. E-mail: sunqf@pku.edu.cn

© 2021 Chinese Physical Society and IOP Publishing Ltd

the zero-energy bound states with non-Abelian statistics, form the degenerate ground state within the gap, which offers the computational space for topological quantum computation.[20] MZMs follow the braiding rule of Ising anyons: after exchanging the positions of two MZMs, one of them acquires a π phase while the other does not, i.e., $\gamma_i \to \gamma_j, \gamma_j \to -\gamma_i$.[19,21] The term "non-Abelian" refers that the braiding of γ_i and γ_j does not commute with the braiding of γ_j and γ_k. MZMs have been proposed as qubits, and the fermion parity of MZMs paired in a certain way is defined as the quantum basis states. Braiding MZMs means exchanging their pairing ways, i.e., rotating the quantum state within the zero-energy degenerate ground state manifold, but keeping the total fermion parity invariant. Due to the global topology, local perturbations do not destroy the ground state, which offers the computational protection as the main advantage but also requires global operations, i.e., the braiding operations, to realize quantum gates corresponding to the Clifford algebra.

Exploring MZMs in theory is both attractive and challenging.[22,23] Kitaev first constructed a toy model containing MZMs as the zero-dimensional end state of a 1D spinless p-wave superconducting nanowire.[24] Despite its difficulty to be realized in experiments, the spinless p-wave superconductor inspires new routines to synthesize the so-called topological superconductor (TSC), which supports MZMs at the boundary or at the vortex. With the development of topological materials[25–28] with strong spin–orbit coupling, Fu and Kane started from a 2D topological insulator, covered it with an s-wave superconductor to induce the pairing potential, and added a ferromagnetic insulator to break the time-reversal symmetry so as to trap MZMs at domain walls.[29,30] MZMs also appear at the end of the 1D nanowire with strong spin–orbit coupling, when applied with a perpendicular magnetic field and covered with an s-wave superconductor.[31–33] MZMs can be induced by a small magnetic field in a hollow nanowire sandwiched between two superconductors.[34] MZMs localize at the vortices in the topological superconducting region when 3D topological insulators or 2D electron gas with Rashba spin–orbit coupling are sandwiched by an s-wave superconductor and a ferromagnetic insulator.[29,35] Besides, Tang *et al.* predicted the existence of the MZMs in some organic molecules (e.g., DNA) proximity coupled by an s-wave superconductor and under the magnetic field.[36]

Considering the experimental detection of MZMs, one of the most important theoretical proposals points out that the existence of MZMs leads to a transport outcome: a robust and quantized zero-bias conductance peak due to the perfect Andreev reflection.[37] Correspondingly, Mourik *et al.* in 2012 first detected the anomalous zero-bias conductance peak as the signature of MZMs locating at the end of the InAs nanowire.[38] After that, other experiments observed MZMs bound at the end of ferromagnetic iron (Fe) atomic chains on the surface of superconducting lead (Pb),[39] the vortex of the iron-based superconductor[40] as well as the interface of the helical hinge states of Bi and magnetic iron clusters on the superconducting substrate.[41] Besides, the 4π periodic fractional Josephson experiment provided compelling evidence of the charge parity conservation of MZMs.[42]

Then the question comes that how to braid MZMs in a real physical system and how to realize the topological quantum computation based on MZMs, facing with the difficulty that MZMs are constrained at the end or vortex of TSCs. The T junctions[43] or Y junctions[44] are theoretically proposed to move the MZM one by one by tuning the electric gate or magnetic flux, changing the topology of superconducting regions, evolving the system from one degenerate ground state to another, or pushing one MZM from one end to another end. During such evolution process, the non-Abelian Berry phase accumulates and one of the two MZMs gets a π phase, after completing the braiding process. Moreover, there is a "strange" strategy named as "braiding without braiding",[45] which does not need to move MZMs but to measure them. When performing a physical measurement on a non-eigen superposition state, this superposition state will collapse into one of the eigenstates, corresponding to a kind of state transformations.[46] Some works based on the electron-teleportation,[47] measuring the fermion parity,[48] and encoding the non-local entanglement of MZMs provide an alternative way of detecting the non-Abelian property and constructing the topologically protected quantum gates.[49] Other issues have also been considered, including the state distillation or the error correction.[50,51] However, based on the braiding of the MZMs, it is difficult to realize the T quantum gate, one of the three universal quantum gates.

As the one-dimensional counterpart of MZMs, chiral Majorana fermions arise as edge states of the 2D TSCs.[52] Theoretical works first predict chiral Majorana fermions in the system of a quantum anomalous Hall insulator (QAHI)[53–55] (or a topological insulator hybrid with ferromagnetic materials) in proximity with s-wave superconductors.[56–58] Generally, the QAHI has chiral edge states of Dirac fermions with Chern number $\mathcal{C} = 1$,[59] which is topologically equivalent to the TSC with $\mathcal{N} = 2$ in the Majorana basis. Via the electric gate or magnetic field, the TSC region can be tuned from the $\mathcal{N} = 1$ topological phase into the trivial superconducting phase with $\mathcal{N} = 0$ or the $\mathcal{N} = 2$ topological phase (QAHI).[60,61] The topological inequivalence between the $\mathcal{N} = 1$ TSC and the $\mathcal{N} = 2$ QAHI produces the chiral Majorana fermion propagating along the boundary. Similar to MZMs, chiral Majorana fermions cannot be directly detected by electric or magnetic fields because of their charge neutrality. Recently, some strategies have been proposed to regulate the phase of chiral

Majorana fermions by the tunneling of the chiral Majorana edge states[62] or the scanning tunneling microscope tip,[63] to control their trajectories by the electric gate[64] or the magnetic flux,[65] etc. These strategies of the regulation lay the foundation for topological quantum computation based on the the chiral Majorana fermions.

A recent experiment, inspired by the theoretical proposal of Ref. [60], reported the measurement of the chiral Majorana fermion and observed the half-integer quantized plateau of the Hall conductance.[66] However, alternative theoretical interpretations of the origin of the half-integer quantized plateau led to a skeptical or supportive attitude to the existence of the chiral Majorana fermion.[67–70] Based on the percolation model of QAHI–superconductor–QAHI junction, Huang *et al.*[67] showed that edge modes could transmit from left to right through the superconducting region with suitable leakage to adjacent chiral edges near the percolation threshold, giving rise to a nearly flat half-integer conductance. Ji and Wen[68] studied the contact conductance under a magnetic field and found that the half-integer conductance is a common result of a good electric contact between the integer quantum Hall insulator and superconductor films. Also, another experiment[71] studied the electric transport of a similar heterostructure of QAHI and s-wave superconductor, and they presented the half-integer quantized conductance without chiral Majorana fermions: two QAHI regions in series with well-aligned magnetization always lead to the half-integer quantized conductance because of the good contact transparency.

Besides the interest in confirming the existence and regulating chiral Majorana fermions, some intuitive ideas turn to braiding chiral Majorana fermions with the purpose of quantum computation. Compared with MZMs, the most exciting property of chiral Majorana fermions is their natural mobility with the potential for rapid information processing. Lian *et al.*[72] first suggested to perform the braiding of chiral Majorana fermions with a Corbino ring junction. Zhou *et al.*[73] proposed the braiding-like operation of chiral Majorana fermions via the quantum dot. In addition, Beenakker *et al.*[74] constructed a device to braid the mobile chiral Majorana vortex around the immobile bulk vortex based on the Josephson junction. Despite these proposals of non-Abelian detections or operations, there is no scheme to implement the universal quantum computation via chiral Majorana fermions, especially the T and CNOT gates.

In this paper, we propose the realization of arbitrary two-qubit quantum gates based on chiral Majorana fermions. Starting from the QAHI–TSC hybrid system, we first construct the elementary cell consisting of a QAHI surrounded by a TSC, which supports two chiral Majorana fermions along the boundary. Then, we introduce an electric gate on the QAHI region and a quantum-dot structure between adjacent cells to braid and partially exchange any two chiral Majorana fermions. Two chiral Majorana fermions in two edge channels within the same cell can be redistributed since the electric gate-induced dynamical phase mixes the electron and hole components. The quantum-dot structure contains two quantum dots, the central one of which allows the quantum tunneling of the chiral Majorana fermions between adjacent cells and the side dot makes up the phase to satisfy the braiding convention. Considering a single qubit defined by four chiral Majorana fermions, the electric gate can tune the trajectory of the chiral Majorana fermions so that half of each incoming chiral Majorana fermion tunnels into the opposite side and the other half keeps its own trajectory, thus realizing an expected T quantum gate. Three braiding operations via two electric gates and one quantum-dot structure achieve an H quantum gate. Based on the minimal definition of two-qubit basis states, we use six chiral Majorana fermions to construct an entangled CNOT quantum gate. Furthermore, the former single-qubit T and H quantum gates are realized within the two-qubit scheme. Besides, we show that a useful quantum Fourier transform algorithm can be decomposed into the aforementioned three quantum gates based on chiral Majorana fermions.

This paper is organized as follows. Section 2 depicts the elementary cell supporting chiral Majorana fermions and explains the function of electric gates and quantum dots to achieve the braiding operation and the partial exchange operation. In Section 3, we construct the quantum gates of the single-qubit and two-qubit gates. In Section 4, a quantum circuit model of the two-qubit quantum Fourier transform is shown with the quantum gates realized via chiral Majorana fermions. We discuss the initialization and measurement of qubits based on chiral Majorana fermions and state the advantage of our proposal in Section 5. We summarize and discuss the further utilization of chiral Majorana fermions in Section 6.

2. Elementary cells for the Braiding and partial exchange operations

In this section, we design the elementary cell to realize the braiding operation and the partial exchange operation of chiral Majorana fermions. The proposed elementary cell consists of a QAHI surrounded by a TSC with electric gates, as shown in Fig. 1(a). Due to the topological inequivalence, one chiral Majorana fermion locates at the boundary between the $\mathcal{N}=1$ TSC region (colored gray) and the $\mathcal{N}=2$ QAHI region (colored yellow), and the other chiral Majorana fermion locates at the boundary between the $\mathcal{N}=1$ TSC region and the vacuum with $\mathcal{N}=0$. Without the electric gate, two chiral Majorana fermions propagate counterclockwise (or clockwise) along the edges of TSC without scattering. An electric gate, i.e., the light blue rectangle in Fig. 1(a), covering the outer side of the

convex QAHI region can regulate the trajectory of two chiral Majorana fermions.[64] The two chiral Majorana fermions along the edges of the TSC before encountering the electric gate are denoted as γ_1 and γ_2. When traveling into the convex QAHI region, they combine into an electron and a hole, $\frac{1}{2}(\gamma_1+\mathrm{i}\gamma_2)=a$ and $\frac{1}{2}(\gamma_1-\mathrm{i}\gamma_2)=a^\dagger$. Through the electric gate region, the electron acquires a dynamical phase $b=\mathrm{e}^{-\mathrm{i}\theta}a$, while the hole gets an opposite phase $b^\dagger=\mathrm{e}^{\mathrm{i}\theta}a^\dagger$. Here the dynamical phase θ could be controlled via the gate voltage.[64] Then, the electron and the hole split again into two chiral Majorana fermions along the edges of the TSC, $b=\frac{1}{2}(\gamma_1'+\mathrm{i}\gamma_2')$ and $b^\dagger=\frac{1}{2}(\gamma_1'-\mathrm{i}\gamma_2')$. To sum up, the electric gate converts the incoming chiral Majorana fermions into the outgoing chiral Majorana fermions via a scattering matrix as follows:

$$\begin{pmatrix}\gamma_1'\\ \gamma_2'\end{pmatrix}=\begin{pmatrix}\cos\theta & \sin\theta\\ -\sin\theta & \cos\theta\end{pmatrix}\begin{pmatrix}\gamma_1\\ \gamma_2\end{pmatrix}. \tag{1}$$

That is, the electric gate can regulate the outgoing trajectory of two incoming chiral Majorana fermions.[64]

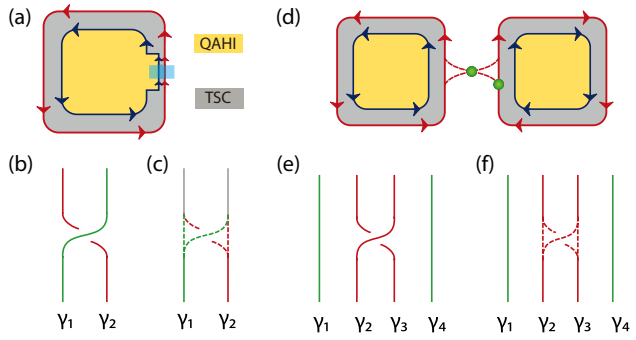


Fig. 1. (a) Schematic diagram of the elementary cell consisting of a QAHI surrounded by a TSC. The yellow and gray regions represent the $\mathcal{N}=2$ QAHI and the $\mathcal{N}=1$ TSC, respectively. Chiral Majorana fermions marked with bold lines propagate along the boundary with arrows denoting the chirality. The electric gate (the light blue rectangle) controls two chiral Majorana fermions in the same cell. The corresponding operation diagrams depict the braiding operation B_{12} in (b) and the partial exchange operation $T_{12}(\theta)$ in (c). (d) A quantum-dot structure with two dots colored green controls two chiral Majorana fermions in two adjacent elementary cells. The corresponding operation diagrams depict the braiding operation B_{23} in (e) and the partial exchange operation $T_{23}(\theta)$ in (f).

The regulation of the electric gate plays important roles in braiding or partially exchanging chiral Majorana fermions. Explicitly, when the gate is closed, i.e., $\theta=0$, the injected chiral Majorana fermions leave straightly. When the gate picks a suitable value such that $\theta=\pi/2$, the scattering matrix gives $\gamma_1'=\gamma_2$ and $\gamma_2'=-\gamma_1$, that is, two chiral Majorana fermions are entirely exchanged, one of which gets an additional π phase. This is exactly a braiding operation. We label an elementary braiding as B_{ij} with the convention $\gamma_i\to\gamma_j,\gamma_j\to-\gamma_i,j=i+1$ and plot the braiding diagram of γ_1 and γ_2 in Fig. 1(b).[21] When the gate voltage is adjusted to produce a dynamic phase which is not an integer multiple of $\pi/2$, $\gamma_1\to\cos\theta\gamma_1+\sin\theta\gamma_2$, $\gamma_2\to-\sin\theta\gamma_1+\cos\theta\gamma_2$, two outgoing chiral Majorana fermions are the mixture of incoming γ_1 and γ_2. Explicitly, a portion of γ_1 propagates along the initial side of TSC while the rest portion jumps into the opposite side of TSC. We name this process, $\gamma_i\to\cos\theta\gamma_i+\sin\theta\gamma_j$ and $\gamma_j\to-\sin\theta\gamma_i+\cos\theta\gamma_j$ with $j=i+1$, as the partial exchange operation of two chiral Majorana fermions, denoted by $T_{ij}(\theta)$. The partial exchange diagram of γ_1 and γ_2 is plotted in Fig. 1(c). Diagrams with solid cross curves in Fig. 1(b) and dashed cross curves in Fig. 1(c) distinguish the braiding process from the partial exchange process under different values of the gate voltage.

Besides the regulation of two chiral Majorana fermions in the same elementary cell, we introduce the quantum-dot structure to braid and partially exchange chiral Majorana fermions between two adjacent elementary cells. Here the magnetization orientations of two adjacent cells are set in the opposite directions, leading to the chirality of the corresponding chiral Majorana fermions being opposite, as shown in Fig. 1(d). As a result, the adjacent chiral Majorana fermions from the adjacent cells have the same mobile direction, which is beneficial for their braiding. A quantum-dot structure of two quantum dots inserts between these two adjacent cells and couples with two adjacent co-propagating chiral Majorana fermions, γ_2 and γ_3. Let us consider the central quantum dot coupling with two chiral Majorana fermions. The Hamiltonian of the chiral Majorana fermions is[73]

$$\mathcal{H}_0=\mathrm{i}v\sum_{m=2,3}\int_{-\infty}^{+\infty}\gamma_m(x)\partial_x\gamma_m(x)\,\mathrm{d}x, \tag{2}$$

where the Majorana operator is Hermitian, $\gamma_m^\dagger(x)=\gamma_m(x)$ and satisfies the anticommutation relation, $\{\gamma_m(x),\gamma_n(x')\}=\delta_{mn}\delta(x-x')$. Then, consider a quantum dot with one single level and the Hamiltonian reads $\mathcal{H}_{\mathrm{QD}}=\epsilon_{\mathrm{d}}d^\dagger d$. The coupling term between chiral Majorana fermions and the quantum dot is $\mathcal{H}_{\mathrm{c}}=\sum_{m=2,3}\mathrm{i}\frac{t_m}{\sqrt{2}}\gamma_m(0)\left(d+d^\dagger\right)$. Thus, the total Hamiltonian is $\mathcal{H}=\mathcal{H}_0+\mathcal{H}_{\mathrm{QD}}+\mathcal{H}_{\mathrm{c}}$.

In the following, we derive the scattering matrix by following the process in Ref. [73]. First, based on the equation of motion of operators in the Heisenberg picture, $\mathrm{i}\partial_t O(t)=[O(t),\mathcal{H}]$, we have

$$\mathrm{i}\partial_t\gamma_m(x,t)=2\mathrm{i}v\partial_x\gamma_m(x,t)+\mathrm{i}\frac{t_m}{\sqrt{2}}\delta(x)\left[d(t)+d^\dagger(t)\right], \tag{3}$$

$$\mathrm{i}\partial_t d(t)=\epsilon_{\mathrm{d}}d(t)-\sum_{m=2,3}\mathrm{i}\frac{t_m}{\sqrt{2}}\gamma_m(0,t), \tag{4}$$

$$\mathrm{i}\partial_t d^\dagger(t)=-\epsilon_{\mathrm{d}}d^\dagger(t)-\sum_{m=2,3}\mathrm{i}\frac{t_m}{\sqrt{2}}\gamma_m(0,t). \tag{5}$$

Then we do the Fourier transform of Eqs. (3)–(5) from the time space to the energy space with $\gamma_m(x,\epsilon)=\int\gamma_m(x,t)\,\mathrm{e}^{\mathrm{i}\epsilon t}\,\mathrm{d}t$. Operators after the Fourier transform are

$$\epsilon\gamma_m(x,\epsilon)=2\mathrm{i}v\partial_x\gamma_m(x,\epsilon)+\mathrm{i}\frac{t_m}{\sqrt{2}}\delta(x)\left[d(\epsilon)+d^\dagger(-\epsilon)\right], \tag{6}$$

$$\epsilon d(\epsilon)=\epsilon_{\mathrm{d}}d(\epsilon)-\sum_{m=2,3}\mathrm{i}\frac{t_m}{\sqrt{2}}\gamma_m(0,\epsilon), \tag{7}$$

$$\epsilon d^{\dagger}(-\epsilon) = -\epsilon_{\rm d} d^{\dagger}(-\epsilon) - \sum_{m=2,3} {\rm i}\frac{t_m}{\sqrt{2}}\gamma_m(0,\epsilon). \tag{8}$$

Integrate x in Eq. (6) from 0^- to 0^+, we get

$$2{\rm i}v\left[\gamma_m(0^+,\epsilon)-\gamma_m(0^-,\epsilon)\right]+{\rm i}\frac{t_m}{\sqrt{2}}\left[d(\epsilon)+d^{\dagger}(-\epsilon)\right]=0. \tag{9}$$

Set $\gamma_m(0,\epsilon)=\frac{1}{2}\left[\gamma_m(0^+,\epsilon)+\gamma_m(0^-,\epsilon)\right]$ and insert Eqs. (7) and (8) into Eq. (9),

$$\gamma_m(0^+,\epsilon)-\gamma_m(0^-,\epsilon)+\frac{t_m}{A}\sum_{n=2,3}t_n\left[\gamma_n(0^+,\epsilon)+\gamma_n(0^-,\epsilon)\right]=0, \tag{10}$$

where $A=4{\rm i}v(\epsilon^2-\epsilon_{\rm d}^2)/\epsilon$, ϵ is the incident energy. Rearrange Eq. (10) to construct the relation between $\gamma_m(0^+,\epsilon)$ and $\gamma_m(0^-,\epsilon)$ as follows:

$$\begin{pmatrix}\gamma_2(0^+,\epsilon)\\ \gamma_3(0^+,\epsilon)\end{pmatrix}=S\begin{pmatrix}\gamma_2(0^-,\epsilon)\\ \gamma_3(0^-,\epsilon)\end{pmatrix}, \tag{11}$$

where S denotes the scattering matrix[73]

$$S=\frac{1}{A+t_2^2+t_3^2}\begin{pmatrix}A+t_3^2-t_2^2 & -2t_2t_3\\ -2t_2t_3 & A+t_2^2-t_3^2\end{pmatrix}. \tag{12}$$

The off-diagonal elements of S represent the tunneling between chiral Majorana fermions γ_2 and γ_3 via a quantum dot. The energy level of a quantum dot can be well tuned by the gate voltage in experiments.[9,75] Consider the incident energy ϵ being very close to zero (Fermi energy) so that the chiral Majorana fermions are with zero energy. When the intra-dot energy level $\epsilon_{\rm d}$ is tuned to be far away from zero, $S\to\begin{pmatrix}1&0\\0&1\end{pmatrix}$, that is, the mismatch of energy disables the quantum dot so γ_2 and γ_3 propagate without tunneling, i.e., no braiding between γ_2 and γ_3. On the other hand, when $\epsilon_{\rm d}=0$, the quantum dot is enabled. In this case, let $t_2=t_3\tan(\theta/2)$, where θ describes the relative value of the coupling strength between chiral Majorana fermions γ_2 and γ_3 with the quantum dot. The purely real scattering matrix of chiral Majorana fermions coupling with a quantum dot is

$$\begin{aligned}S(\epsilon=\epsilon_{\rm d},\theta)&=\frac{1}{t_2^2+t_3^2}\begin{pmatrix}t_3^2-t_2^2 & -2t_2t_3\\ -2t_2t_3 & t_2^2-t_3^2\end{pmatrix}\\&=\begin{pmatrix}\cos\theta & -\sin\theta\\ -\sin\theta & -\cos\theta\end{pmatrix}.\end{aligned} \tag{13}$$

Comparing Eqs. (13) and (1), there still exists a π phase difference. According to Eq. (13), θ, the relative value of the coupling strength between chiral Majorana fermions with the quantum dot, determines the mixing ratio of the incoming chiral Majorana fermions. When $\theta=0$, i.e., $t_2=0$, the scattering matrix equals $\begin{pmatrix}1&0\\0&-1\end{pmatrix}$. Here, the quantum dot is just coupled to one chiral Majorana fermion γ_3, resulting in an additional phase π to γ_3.[63,73] Thus, we add another quantum dot [see Fig. 1(d)] only coupled to γ_3 to compensate the phase π (negative sign) of the difference between Eqs. (13) and (1). So the scattering matrix of the quantum-dot structure as shown in Fig. 1(d) is derived as

$$S_2(\theta)=S(\epsilon=\epsilon_{\rm d},\theta)\begin{pmatrix}1&0\\0&-1\end{pmatrix}=\begin{pmatrix}\cos\theta & \sin\theta\\ -\sin\theta & \cos\theta\end{pmatrix}, \tag{14}$$

matching the scattering matrix via the electric gate in Eq. (1). When $\theta=0$, the disabled quantum-dot structure has no effect on the chiral Majorana fermions. When $\theta=\pi/2$, here comes $\gamma_2\to\gamma_3$ and $\gamma_3\to-\gamma_2$, that is, the enabled quantum-dot structure completes the braiding operation B_{23}, shown in Fig. 1(e). When the relative coupling is tuned to a suitable value, the quantum-dot structure performs the partial exchange operation $T_{23}(\theta)$: $\gamma_2\to\cos\theta\gamma_2+\sin\theta\gamma_3$ and $\gamma_3\to-\sin\theta\gamma_2+\cos\theta\gamma_3$, as shown in Fig. 1(f).

Based on the braiding operation implemented via an electric gate or a quantum-dot structure, we further introduce a transfer box to connect two vertically adjacent elementary cells, as shown in Fig. 2(a). Figure 2(b) draws a symbolic picture of a transfer box with four chiral Majorana fermions injecting and ejecting. The transfer box contains two electric gates and two quantum-dot structures arranged in the way shown in Fig. 2(c). If the electric gates and quantum dots are disabled, the transfer box is closed, so four chiral Majorana fermions propagate in their own way, $(\gamma_1,\gamma_2,\gamma_3,\gamma_4)\to(\gamma_1,\gamma_2,\gamma_3,\gamma_4)$, i.e., the chiral Majorana pair γ_1 and γ_2 remains in the upper cell and the pair γ_3 and γ_4 remains in the lower cell. But when the electric gates and quantum dots are tuned to the value corresponding to $\theta=\pi/2$, the transfer box is open and executes the braiding operations B_{23}, B_{12}, B_{34}, and B_{23} in series. To be specific, four chiral Majorana fermions transform as follows:

$$\begin{aligned}(\gamma_1,\gamma_2,\gamma_3,\gamma_4)&\to(\gamma_1,\gamma_3,-\gamma_2,\gamma_4)\to(\gamma_3,-\gamma_1,\gamma_4,\gamma_2)\\&\to(\gamma_3,\gamma_4,\gamma_1,\gamma_2).\end{aligned} \tag{15}$$

Thus, Fig. 2(d) clearly shows the function of a transfer box: carry out four braiding operations, exchange of the Majorana pair γ_1 and γ_2 with the pair γ_3 and γ_4, and transfer the Majorana

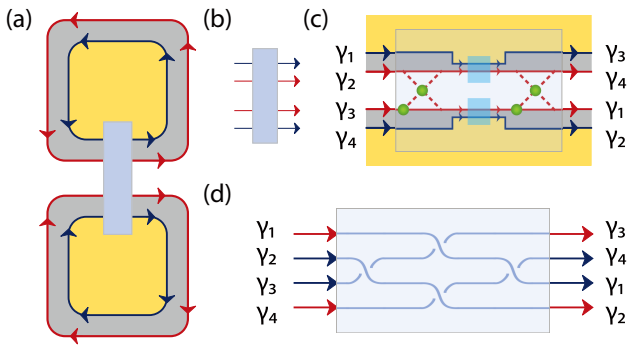


Fig. 2. (a) Schematic diagram of two vertically adjacent elementary cells with a transfer box between them. (b) Symbolic picture of the transfer box. (c) The detailed structure of the transfer box with two electric gates and two quantum-dot structures. (d) Braiding diagram of operations B_{23}, B_{12}, B_{34}, and B_{23}, depicting the function of the transfer box as transferring the Majorana pair from the lower cell to the upper cell.

pair γ_3 and γ_4 from the lower cell to the upper cell. This transfer makes possible cascading vertical cells and braiding chiral Majorana fermions on both sides to be seen in Fig. 6.

3. Realization of quantum gates

A complete quantum computation process includes three parts: input the qubit, perform the quantum gate operation, and read out the final qubit. The core of quantum computation lies in the realization of arbitrary quantum gates. The standard set of universal quantum gates is {H, T, CNOT}, specifically,

$$\mathrm{H}=\frac{1}{\sqrt{2}}\begin{pmatrix}1 & 1\\ 1 & -1\end{pmatrix},\ \mathrm{T}=\begin{pmatrix}1 & 0\\ 0 & \mathrm{e}^{\mathrm{i}\frac{\pi}{4}}\end{pmatrix},\ \mathrm{CNOT}=\begin{pmatrix}1&0&0&0\\0&1&0&0\\0&0&0&1\\0&0&1&0\end{pmatrix}. \tag{16}$$

Considering the quantum states as qubits, the essence of the quantum gate is the unitary operation in the Hilbert space. In this section, we utilize chiral Majorana fermions as the qubit, use the electric gate and the quantum-dot structure to perform operations on the qubit, and construct the quantum gates in the two-qubit basis to realize any two-qubit quantum operations.

Recalling the elementary cell device in Section 2, we have realized the braiding operation of adjacent chiral Majorana fermions via an electric gate or a quantum-dot structure. Here, we denote the braiding operator of Majorana fermions as[21]

$$B_{i,i+1}:\ \gamma_i\to\gamma_{i+1},\ \gamma_{i+1}\to-\gamma_i. \tag{17}$$

Express the operator in terms of the bilinear Majorana operators as follows:

$$B_{i,i+1}=\frac{1}{\sqrt{2}}(1+\gamma_{i+1}\gamma_i), \tag{18}$$

$$B^{-1}_{i,i+1}=\frac{1}{\sqrt{2}}(1+\gamma_i\gamma_{i+1}). \tag{19}$$

The operators $B_{i,i+1}$ and $B^{-1}_{i,i+1}$ satisfy $B^{\dagger}_{i,i+1}=B^{-1}_{i,i+1}$, $B_{i,i+1}\gamma_i B^{-1}_{i,i+1}=\gamma_{i+1}$, and $B_{i,i+1}\gamma_{i+1}B^{-1}_{i,i+1}=-\gamma_i$.

Similarly, for the partial exchange operation, we denote the operator as $T_{i,i+1}(\theta)$,

$$T_{i,i+1}(\theta):\ \gamma_i\to\cos\theta\gamma_i+\sin\theta\gamma_{i+1},\ \gamma_{i+1}\to-\sin\theta\gamma_i+\cos\theta\gamma_{i+1}, \tag{20}$$

and express $T_{i,i+1}(\theta)$ in terms of the bilinear Majorana operators

$$T_{i,i+1}(\theta)=\cos\frac{\theta}{2}+\sin\frac{\theta}{2}\gamma_{i+1}\gamma_i, \tag{21}$$

$$T^{-1}_{i,i+1}(\theta)=\cos\frac{\theta}{2}+\sin\frac{\theta}{2}\gamma_i\gamma_{i+1}, \tag{22}$$

which satisfies

$$\begin{aligned}T_{i,i+1}(\theta)\gamma_i T^{-1}_{i,i+1}(\theta)&=\cos\theta\gamma_i+\sin\theta\gamma_{i+1},\\ T_{i,i+1}(\theta)\gamma_{i+1}T^{-1}_{i,i+1}(\theta)&=-\sin\theta\gamma_i+\cos\theta\gamma_{i+1}.\end{aligned} \tag{23}$$

When $\theta=0$, $T_{i,i+1}(0)=1$. When $\theta=\pi/2$, $T_{i,i+1}(\pi/2)=B_{i,i+1}$, i.e., the braiding operation represents the total exchange with a dynamical phase being $\pi/2$ or equal coupling between the quantum dot and two chiral Majorana fermions.

Hereafter, we regard the braiding operator $B_{i,i+1}$ and the partial exchange operator $T_{i,i+1}(\theta)$ (θ is not an integer multiple of $\pi/2$) as the elementary operations of two chiral Majorana fermions to construct the quantum gates.

3.1. The single-qubit T and H gates

For a single qubit, the minimal number of Majorana fermions is four, due to the fermion parity conservation.[21,76] Thus we place two column of elementary cells to construct the single-qubit quantum device, as shown in Figs. 3(a) and 4(a). Four Majorana fermions are input from the lower cells A1 and A2, conveyed via two transfer boxes to the cells B1 and B2, acted on by the quantum operations in the cells B1 and B2, conveyed via two transfer boxes to the cells C1 and C2 as the output. As for the quantum gate, we focus on the core cells B1 and B2 with four incoming chiral Majorana fermions propagating upward, denoted as γ_1, γ_2, γ_3, and γ_4 from left to right.

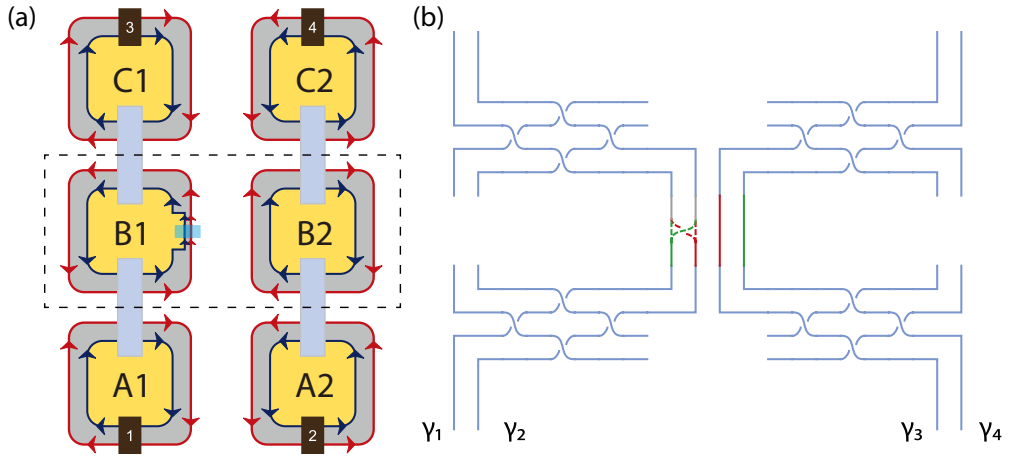


Fig. 3. Construction of the T gate. (a) The single qubit device contains two columns of elementary cells supporting four chiral Majorana fermions. The dashed rectangle emphasizes the core region which performs the T gate with an electric gate. (b) Braiding diagram of operations in (a). The dashed cross line represents the partial exchange operation of γ_1 and γ_2, $T_{1,2}(\pi/4)$, leading to the transformation of chiral Majorana fermions in Eq. (35).

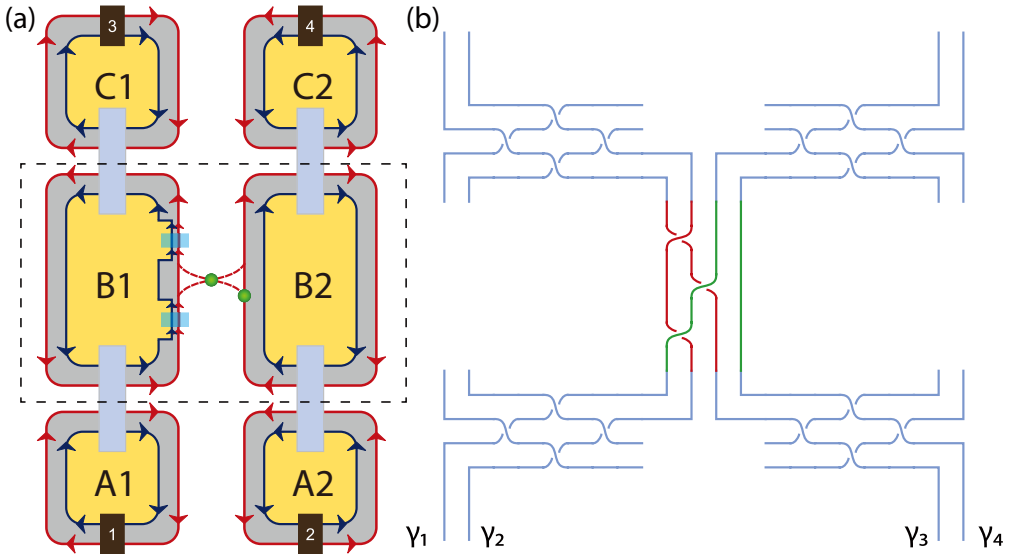


Fig. 4. Construction of the H gate. (a) The single qubit device contains two columns of elementary cells supporting four chiral Majorana fermions. The dashed rectangle emphasizes the core region which performs the H gate with two electric gates and one quantum-dot structure. (b) Braiding diagram of operations in (a). The central cross lines represent the braiding operations of B_{12}, B_{23}, and B_{12} in series, leading to the transformation of chiral Majorana fermions in Eq. (37).

Based on the relation between the Dirac fermion and the Majorana fermion, $\psi_{\rm L}=\frac{1}{2}(\gamma_1+{\rm i}\gamma_2)$ and $\psi_{\rm R}=\frac{1}{2}(\gamma_3+{\rm i}\gamma_4)$, we define the quantum basis states in terms of the fermion occupation number as follows:

$$|00\rangle=|0\rangle_{\rm L}\otimes|0\rangle_{\rm R}=|{\rm vac}\rangle\,, \tag{24}$$

$$|10\rangle=|1\rangle_{\rm L}\otimes|0\rangle_{\rm R}=\psi_{\rm L}^{\dagger}|{\rm vac}\rangle\,, \tag{25}$$

$$|01\rangle=|0\rangle_{\rm L}\otimes|1\rangle_{\rm R}=\psi_{\rm R}^{\dagger}|{\rm vac}\rangle\,, \tag{26}$$

$$|11\rangle=|1\rangle_{\rm L}\otimes|1\rangle_{\rm R}=\psi_{\rm L}^{\dagger}\psi_{\rm R}^{\dagger}|{\rm vac}\rangle\,, \tag{27}$$

where $|{\rm vac}\rangle$ represents the vacuum state satisfying $\psi_\alpha|{\rm vac}\rangle=0$ and $\psi_\alpha^{\dagger}|{\rm vac}\rangle=|1\rangle_\alpha$, $\alpha={\rm L,R}$.

Under the basis $(|00\rangle,|10\rangle,|01\rangle,|11\rangle)$, we derive the matrix form of the partial exchange operator $T_{i,i+1}(\theta)$. If γ_i and γ_{i+1} belong to the same elementary cell of which Dirac fermions are labeled as $\psi_\alpha^{\dagger}$ and ψ_α, then

$$T_{i,i+1}(\theta)=\cos\frac{\theta}{2}+{\rm i}\sin\frac{\theta}{2}\left(2\psi_\alpha^{\dagger}\psi_\alpha-1\right), \tag{28}$$

$$\begin{aligned}T_{i,i+1}(\theta)|0\rangle_\alpha&={\rm e}^{-{\rm i}\frac{\theta}{2}}|0\rangle_\alpha\,,\\ T_{i,i+1}(\theta)|1\rangle_\alpha&={\rm e}^{+{\rm i}\frac{\theta}{2}}|1\rangle_\alpha\,,\end{aligned} \tag{29}$$

that is, $T_{i,i+1}(\theta)$ only acts on the subspace spanned by $|0\rangle_\alpha$ and $|1\rangle_\alpha$ but does nothing on other subspace. But if γ_i and γ_{i+1} belong to different cells, such as $\gamma_2=-{\rm i}\left(\psi_{\rm L}-\psi_{\rm L}^{\dagger}\right)$ and $\gamma_3=\psi_{\rm R}+\psi_{\rm R}^{\dagger}$, then

$$T_{23}(\theta)=\cos\frac{\theta}{2}+{\rm i}\sin\frac{\theta}{2}\left(\psi_{\rm L}-\psi_{\rm L}^{\dagger}\right)\left(\psi_{\rm R}+\psi_{\rm R}^{\dagger}\right), \tag{30}$$

$$\begin{aligned}T_{23}(\theta)|00\rangle&=\cos\frac{\theta}{2}|00\rangle-{\rm i}\sin\frac{\theta}{2}|11\rangle\,,\\ T_{23}(\theta)|11\rangle&=\cos\frac{\theta}{2}|11\rangle-{\rm i}\sin\frac{\theta}{2}|00\rangle\,,\\ T_{23}(\theta)|10\rangle&=\cos\frac{\theta}{2}|10\rangle-{\rm i}\sin\frac{\theta}{2}|01\rangle\,,\\ T_{23}(\theta)|01\rangle&=\cos\frac{\theta}{2}|01\rangle-{\rm i}\sin\frac{\theta}{2}|10\rangle\,.\end{aligned} \tag{31}$$

$$\begin{aligned}T_{23}(\theta)|00\rangle&=\cos\frac{\theta}{2}|00\rangle-{\rm i}\sin\frac{\theta}{2}|11\rangle\,,\\ T_{23}(\theta)|11\rangle&=\cos\frac{\theta}{2}|11\rangle-{\rm i}\sin\frac{\theta}{2}|00\rangle\,,\\ T_{23}(\theta)|10\rangle&=\cos\frac{\theta}{2}|10\rangle-{\rm i}\sin\frac{\theta}{2}|01\rangle\,,\\ T_{23}(\theta)|01\rangle&=\cos\frac{\theta}{2}|01\rangle-{\rm i}\sin\frac{\theta}{2}|10\rangle\,.\end{aligned} \tag{32}$$

Apparently, the partial exchange operation $T_{i,i+1}(\theta)$ keeps the fermion parity of the quantum state, so we define the computational basis of the single qubit with an even fermion parity, $|\mathbf{0}\rangle=|00\rangle,|\mathbf{1}\rangle=|11\rangle$. Under the single-qubit basis $(|\mathbf{0}\rangle,|\mathbf{1}\rangle)$, the matrix form of the partial exchange operator is

$$\begin{aligned}\rho_{\rm s}\left[T_{12}(\theta)\right]&=\begin{pmatrix}{\rm e}^{-{\rm i}\frac{\theta}{2}}&0\\0&{\rm e}^{{\rm i}\frac{\theta}{2}}\end{pmatrix},\\ \rho_{\rm s}\left[T_{23}(\theta)\right]&=\begin{pmatrix}\cos\frac{\theta}{2}&-{\rm i}\sin\frac{\theta}{2}\\-{\rm i}\sin\frac{\theta}{2}&\cos\frac{\theta}{2}\end{pmatrix},\\ \rho_{\rm s}\left[T_{34}(\theta)\right]&=\begin{pmatrix}{\rm e}^{-{\rm i}\frac{\theta}{2}}&0\\0&{\rm e}^{{\rm i}\frac{\theta}{2}}\end{pmatrix}.\end{aligned} \tag{33}$$

Since $B_{i,i+1}=T_{i,i+1}(\pi/2)$, here comes the matrix form of the braiding operator

$$\begin{aligned}&\rho_{\rm s}\left[B_{12}\right]={\rm e}^{-{\rm i}\frac{\pi}{4}}\begin{pmatrix}1&0\\0&{\rm i}\end{pmatrix},\ \rho_{\rm s}\left[B_{23}\right]=\frac{1}{\sqrt{2}}\begin{pmatrix}1&-{\rm i}\\-{\rm i}&1\end{pmatrix},\\ &\rho_{\rm s}\left[B_{34}\right]={\rm e}^{-{\rm i}\frac{\pi}{4}}\begin{pmatrix}1&0\\0&{\rm i}\end{pmatrix}.\end{aligned} \tag{34}$$

Now we construct the T quantum gate performed on the single qubit composed of four chiral Majorana fermions. The T quantum gate can not be realized by the braiding of MZMs. As shown in Fig. 3(a), a gate voltage is applied to the electric gate in the convex QAHI region along the right edge of the elementary cell B1. Tune the gate voltage to achieve the partial exchange operation of chiral Majorana fermions γ_1 and γ_2 with $\theta=\pi/4$, so that one half of the incoming chiral Majorana fermion γ_1 (γ_2) stays in the original path while the other half of γ_1 (γ_2) crosses over and merges into the opposite side [see the dashed crossing curves in Fig. 3(b)]. Follow the definition of the operator $T_{12}(\pi/4)$ in Eq. (20), four chiral Majorana fermions transform as follows:

$$(\gamma_1,\gamma_2,\gamma_3,\gamma_4)\to\left(\cos\frac{\pi}{4}\gamma_1+\sin\frac{\pi}{4}\gamma_2,-\sin\frac{\pi}{4}\gamma_1+\cos\frac{\pi}{4}\gamma_2,\gamma_3,\gamma_4\right). \tag{35}$$

Correspondingly, the single-qubit state basis evolves

$$|\mathbf{0}\rangle \to |\mathbf{0}\rangle, \quad |\mathbf{1}\rangle \to \mathrm{e}^{\mathrm{i}\frac{\pi}{4}}|\mathbf{1}\rangle, \tag{36}$$

based on the matrix form of the partial exchange operator in Eq. (33). Compared with the definition in Eq. (16), the gate-induced partial exchange operation does realize the T quantum gate of chiral Majorana fermions up to a negligible overall phase, since only the relative phase δ of a qubit $|0\rangle + \mathrm{e}^{\mathrm{i}\delta}|1\rangle$ is meaningful.[77]

Then we construct the H quantum gate. Via combining the braiding operations in Eq. (34), the H gate could be decomposed into three braiding operations B_{12}, B_{23}, and B_{12} in series, up to an overall phase.[49,78] We introduce two electric gates to braid chiral Majorana fermions within the elementary cell B1 and one quantum-dot structure to braid between cells B1 and B2, as shown in Fig. 4(a), that is,

$$\begin{aligned}(\gamma_1,\gamma_2,\gamma_3,\gamma_4) &\to (\gamma_2,-\gamma_1,\gamma_3,\gamma_4) \to (\gamma_2,\gamma_3,\gamma_1,\gamma_4)\\ &\to (\gamma_3,-\gamma_2,\gamma_1,\gamma_4).\end{aligned} \tag{37}$$

Correpondingly, the single-qubit state basis evolves

$$|\mathbf{0}\rangle \to \frac{1}{\sqrt{2}}(|\mathbf{0}\rangle + |\mathbf{1}\rangle), \quad |\mathbf{1}\rangle \to \frac{1}{\sqrt{2}}(|\mathbf{0}\rangle - |\mathbf{1}\rangle), \tag{38}$$

which is indeed the unitary transformation under the H gate with the definition in Eq. (16).

3.2. The two-qubit CNOT gate

For the two-qubit state, the minimal number of Majorana fermions is six. Thus, we align three columns of elementary cells as shown in Fig. 5(a). By means of the transfer box to convey the input and output states, we focus on the core cells performing the two-qubit quantum gate, labeled as B1, B2, and B3. Six chiral Majorana fermions move upwards with labels $\gamma_i, i = 1,\ldots,6$ and the corresponding Dirac fermions are denoted as $\psi_{\mathrm{L}} = \frac{1}{2}(\gamma_1 + \mathrm{i}\gamma_2)$, $\psi_{\mathrm{M}} = \frac{1}{2}(\gamma_3 + \mathrm{i}\gamma_4)$, and $\psi_{\mathrm{R}} = \frac{1}{2}(\gamma_5 + \mathrm{i}\gamma_6)$. Then we write four basis states with an even fermion parity as follows:[76]

$$|\mathbf{00}\rangle = |0\rangle_{\mathrm{L}}|0\rangle_{\mathrm{M}}|0\rangle_{\mathrm{R}} = |\mathrm{vac}\rangle, \tag{39}$$

$$|\mathbf{01}\rangle = |0\rangle_{\mathrm{L}}|1\rangle_{\mathrm{M}}|1\rangle_{\mathrm{R}} = \psi_{\mathrm{M}}^{\dagger}\psi_{\mathrm{R}}^{\dagger}|\mathrm{vac}\rangle, \tag{40}$$

$$|\mathbf{10}\rangle = |1\rangle_{\mathrm{L}}|1\rangle_{\mathrm{M}}|0\rangle_{\mathrm{R}} = \psi_{\mathrm{L}}^{\dagger}\psi_{\mathrm{M}}^{\dagger}|\mathrm{vac}\rangle, \tag{41}$$

$$|\mathbf{11}\rangle = |1\rangle_{\mathrm{L}}|0\rangle_{\mathrm{M}}|1\rangle_{\mathrm{R}} = \psi_{\mathrm{L}}^{\dagger}\psi_{\mathrm{R}}^{\dagger}|\mathrm{vac}\rangle, \tag{42}$$

where the central qubit labeled by M serves as the ancillary qubit to balance the fermion parity.

Under the two-qubit basis $(|\mathbf{00}\rangle, |\mathbf{01}\rangle, |\mathbf{10}\rangle, |\mathbf{11}\rangle)$, we derive the matrix form $\rho_{\mathrm{t}}[B_{i,i+1}]$ of the braiding operator $B_{i,i+1}, i = 1,\ldots,5$,

$$\rho_{\mathrm{t}}[B_{12}] = \mathrm{e}^{-\mathrm{i}\frac{\pi}{4}}\begin{pmatrix}1 & 0\\ 0 & \mathrm{i}\end{pmatrix}\otimes I_2, \quad \rho_{\mathrm{t}}[B_{23}] = \frac{1}{\sqrt{2}}\begin{pmatrix}1 & -\mathrm{i}\\ -\mathrm{i} & 1\end{pmatrix}\otimes I_2, \tag{43}$$

$$\rho_{\mathrm{t}}[B_{45}] = I_2 \otimes \frac{1}{\sqrt{2}}\begin{pmatrix}1 & -\mathrm{i}\\ -\mathrm{i} & 1\end{pmatrix}, \quad \rho_{\mathrm{t}}[B_{56}] = I_2 \otimes \mathrm{e}^{-\mathrm{i}\frac{\pi}{4}}\begin{pmatrix}1 & 0\\ 0 & \mathrm{i}\end{pmatrix}, \tag{44}$$

where I_2 is a 2-by-2 identity matrix. These four matrices are not entangled since they can be decomposed into the direct product of single-qubit matrices.[1] However, considering the braiding operator of γ_3 and γ_4, the matrix form is derived as follows:

$$B_{34} = \frac{1}{\sqrt{2}}(1 + \gamma_4\gamma_3) = \frac{1}{\sqrt{2}}\left[1 + \mathrm{i}\left(2\psi_{\mathrm{M}}^{\dagger}\psi_{\mathrm{M}} - 1\right)\right], \tag{45}$$

then $B_{34}|\mathbf{00}\rangle = \mathrm{e}^{-\mathrm{i}\frac{\pi}{4}}|\mathbf{00}\rangle$, $B_{34}|\mathbf{01}\rangle = \mathrm{e}^{\mathrm{i}\frac{\pi}{4}}|\mathbf{01}\rangle$, $B_{34}|\mathbf{10}\rangle = \mathrm{e}^{\mathrm{i}\frac{\pi}{4}}|\mathbf{10}\rangle$, and $B_{34}|\mathbf{11}\rangle = \mathrm{e}^{-\mathrm{i}\frac{\pi}{4}}|\mathbf{11}\rangle$. So we can have

$$\rho_{\mathrm{t}}[B_{34}] = \begin{pmatrix}\mathrm{e}^{-\mathrm{i}\frac{\pi}{4}} & 0 & 0 & 0\\ 0 & \mathrm{e}^{\mathrm{i}\frac{\pi}{4}} & 0 & 0\\ 0 & 0 & \mathrm{e}^{\mathrm{i}\frac{\pi}{4}} & 0\\ 0 & 0 & 0 & \mathrm{e}^{-\mathrm{i}\frac{\pi}{4}}\end{pmatrix}. \tag{46}$$

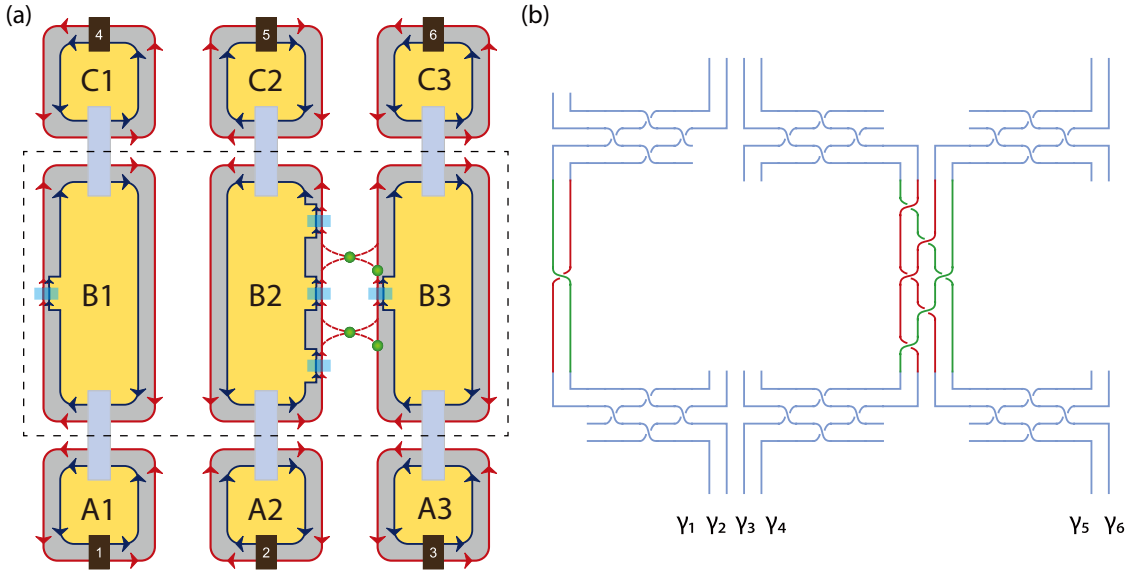


Fig. 5. Construction of the CNOT gate. (a) The two-qubit device contains three columns of elementary cells supporting six chiral Majorana fermions. The dashed rectangle emphasizes the core region which performs the CNOT gate with five electric gates and two quantum-dot structures. (b) Braiding diagram of operations in (a). The central cross lines represent the braiding operations of B_{34}, B_{45}, B_{56}, B_{12}^{-1}, B_{34}, B_{45}, B_{34} in series, leading to the transformation of chiral Majorana fermions in Eq. (48). Note here the B_{12}^{-1} is the inverse braiding of γ_1 and γ_2, realized by an opposite value of the gate voltage corresponding to B_{12}.

Noticeably, the braiding operator B_{34} is an entangled operator since the matrix $\rho_t[B_{34}]$ cannot be decomposed in the direct product form.

The entangled operator is vital in the quantum computation since it introduces the entanglement into the quantum state. One of the famous entangled quantum gates is the CNOT gate (the controlled-NOT gate) performing a conditional operation on the two-qubit state [see the matrix form of CNOT gate in Eq. (16)]. After a CNOT gate, the control qubit remains while the target qubit transforms according to the state of the control qubit: if the control qubit is 1, the target qubit reverses its state; if the control qubit is 0, the target qubit keeps its state.

Combining the basic braiding operators in two-qubit basis, the CNOT gate is decomposed into seven braiding operations up to an overall phase as follows:[76]

$$\text{CNOT} \cong \rho_t\left[B_{34}B_{45}B_{34}B_{12}^{-1}B_{56}B_{45}B_{34}\right]. \tag{47}$$

We construct a device to realize the CNOT gate via five electric gates and two quantum-dot structures, as shown in Fig. 5(a). The effect of seven braiding operations from Eq. (47) in series on the six chiral Majorana fermions of cells B1, B2, and B3 is

$$\begin{aligned}&(\gamma_1,\gamma_2,\gamma_3,\gamma_4,\gamma_5,\gamma_6)\\ &\to(\gamma_1,\gamma_2,\gamma_4,-\gamma_3,\gamma_5,\gamma_6)\to(\gamma_1,\gamma_2,\gamma_4,\gamma_5,\gamma_3,\gamma_6)\\ &\to(\gamma_1,\gamma_2,\gamma_4,\gamma_5,\gamma_6,-\gamma_3)\to(-\gamma_2,\gamma_1,\gamma_4,\gamma_5,\gamma_6,-\gamma_3)\\ &\to(-\gamma_2,\gamma_1,\gamma_5,-\gamma_4,\gamma_6,-\gamma_3)\to(-\gamma_2,\gamma_1,\gamma_5,\gamma_6,\gamma_4,-\gamma_3)\\ &\to(-\gamma_2,\gamma_1,\gamma_6,-\gamma_5,\gamma_4,-\gamma_3),\end{aligned} \tag{48}$$

with the braiding diagram shown in Fig. 5(b). Note that the different crossing direction of γ_1 and γ_2 denotes the inverse braiding operation B_{12}^{-1}. Since $B_{12}^4=1$, $B_{12}^{-1}=B_{12}^3$, the inverse braiding of γ_1 and γ_2 can be realized through three B_{12} operations. Besides, considering the physical realization of the braiding operator in Eq. (1), inversing the gate voltage of the electric gate on B1 can also inverse the braiding. Thus, in Fig. 5(a), we just use one gate to achieve the operator B_{12}^{-1}.

3.3. The T and H gates in the two-qubit basis

In the former subsections, we have constructed the single-qubit T gate and H gate and the two-qubit CNOT gate. In order to complete the set of quantum gates acting on the two-qubit state, we also figure out the T and H gates in the two-qubit basis. In the Hilbert space spanned by six chiral Majorana fermions, the two-qubit basis denoted in Eqs. (39)–(42) can be viewed as the direct product of the computational qubit basis $|\rangle_L$ and $|\rangle_R$, so we can well define the single-qubit operation in the two-qubit basis, i.e., $\mathrm{H_L}=\mathrm{H}\otimes I_2$, $\mathrm{H_R}=I_2\otimes\mathrm{H}$, $\mathrm{T_L}=\mathrm{T}\otimes I_2$, $\mathrm{T_R}=I_2\otimes\mathrm{T}$.

To realize the H gate on the left qubit $\mathrm{H_L}$, we construct the device as shown in Fig. 6(a). Two cells, B4 and B5, are crucial to perform the $\mathrm{H_L}$ gate. Two electric gates and

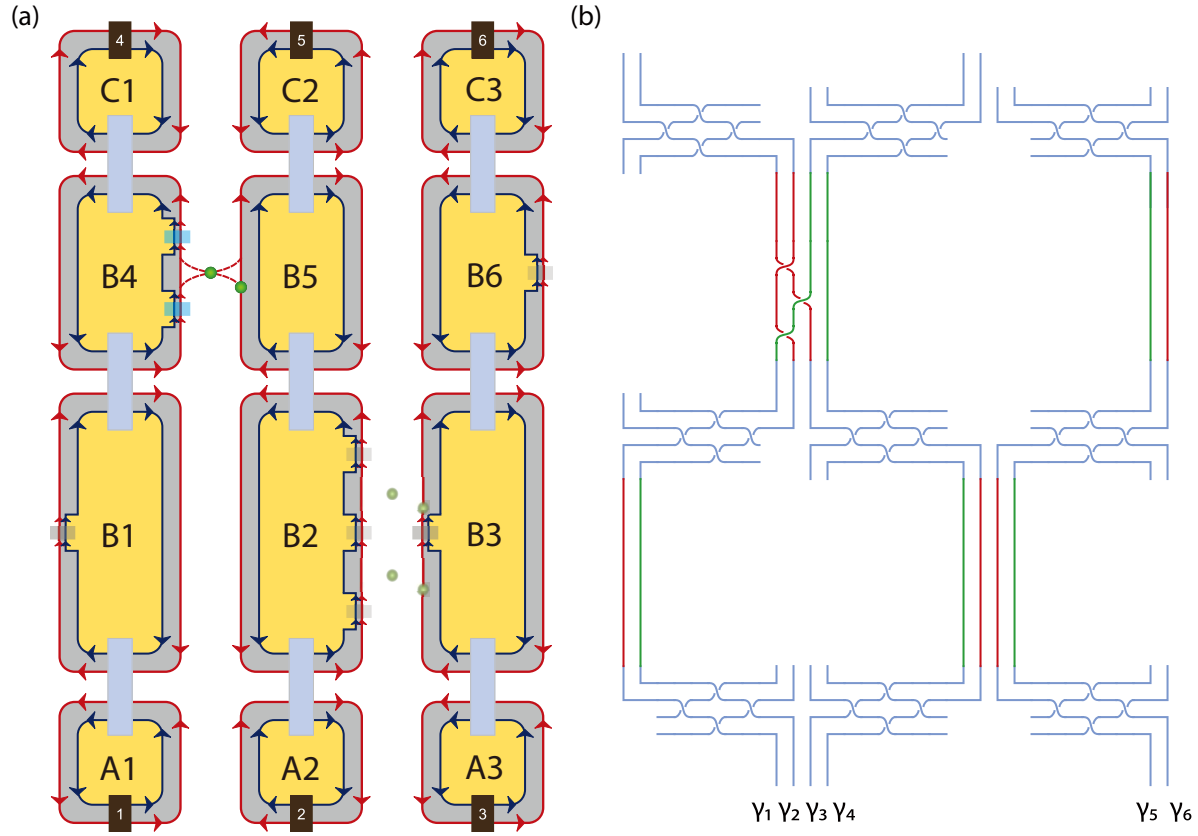


Fig. 6. H gate acting on the left qubit in the two-qubit basis. (a) The two-qubit device contains three columns of elementary cells supporting six chiral Majorana fermions. The colorful electric gates and quantum dots are enabled while the gray ones are disabled. The H gate acting on the left qubit is realized when opening electric gates and quantum dots of cells B4 and B5. Besides, other single-qubit gates or CNOT gate can be realized when enabling other cells in the same was as core regions in Figs. 3–5. (b) Braiding diagram of operations in (a). The central cross lines represent the braiding operations of B_{12}, B_{23} and B_{12} in series, leading to the same transformation of chiral Majorana fermions in Eq. (37).

one quantum-dot structure achieve the braiding operations B_{12}, B_{23}, and B_{12}. Multiplying the matrices of these operators in Eq. (43) gives the H_L gate up to an overall phase,

$$\rho_t[B_{12}B_{23}B_{12}] \cong H_L. \tag{49}$$

Correspondingly, Fig. 6(b) depicts the braiding of γ_1 and γ_2, γ_2 and γ_3, γ_1 and γ_2 in series.

In addition, quantum gates H_R, T_L, and T_R can also be realized via the device in Fig. 6(a). To realize $H_R \cong \rho_t[B_{45}B_{56}B_{45}]$, first disable the electric gates and quantum dots of cells B4 and B5, and then tune the electric gates and quantum dots of cells B2 and B3 in the same way as the dashed rectangular core region plotted in Fig. 4(a). Express the partial exchange operations in the two-qubit basis, such as, $T_{12}\left(\frac{\pi}{4}\right) = \begin{pmatrix} e^{-i\frac{\pi}{8}} & 0 \\ 0 & e^{i\frac{\pi}{8}} \end{pmatrix} \otimes I_2$ and $T_{56}\left(\frac{\pi}{4}\right) = I_2 \otimes \begin{pmatrix} e^{-i\frac{\pi}{8}} & 0 \\ 0 & e^{i\frac{\pi}{8}} \end{pmatrix}$. With the electric gates and quantum dots of cells B4 and B5 disabled, tuning the electric gate of cell B1 (B6) can partially exchange γ_1 and γ_2 (γ_5 and γ_6) so as to realize the gate T_L (T_R).

Based on quantum gates H_L, H_R, T_L, and T_R, all non-entangled single-qubit gates could be achieved. Easily to see, the CNOT gate is compatible with the device in Fig. 6(a). Combined with H_L, H_R, T_L, T_R, and CNOT, arbitrary two-qubit gate can be constructed. Thus, the device plotted in Fig. 6(a) can perform arbitrary two-qubit quantum gate based on six chiral Majorana fermions.

4. The quantum circuit of the quantum Fourier transform

After the realization of quantum gates T, H, and CNOT, as an example, we state that the algorithm of quantum Fourier transform (QFT) can be realized via the two-qubit device of chiral Majorana fermions shown in Fig. 6(a).

Suppose the input state is $|\Psi_{in}\rangle = |x_2\rangle \otimes |x_1\rangle$, with $x_1, x_2 = 0, 1$. The circuit of two-qubit QFT is plotted in Fig. 7(a).[77] Apply one H gate on the first qubit so as to obtain $|\Psi_1\rangle = H_L|\Psi_{in}\rangle = |x_2\rangle \otimes \frac{1}{\sqrt{2}}(|0\rangle + (-1)^{x_1}|1\rangle)$. Define the single-qubit gate $S = \begin{pmatrix} 1 & 0 \\ 0 & e^{i\frac{\pi}{2}} \end{pmatrix}$ and the controlled-S gate is $CS = \begin{pmatrix} I_2 & O \\ O & S \end{pmatrix}$. If we set the second qubit as the control bit and the first qubit as the target bit, after the CS gate, the quantum state becomes $|\Psi_2\rangle = CS|\Psi_1\rangle = |x_2\rangle \otimes \frac{1}{\sqrt{2}}\left(|0\rangle + e^{i\pi x_1 + i\pi x_2/2}|1\rangle\right)$. Then by applying one H gate on the first qubit, the output state is $|\Psi_{out}\rangle = H_R|\Psi_2\rangle = \frac{1}{\sqrt{2}}(|0\rangle + (-1)^{x_2}|1\rangle) \otimes \frac{1}{\sqrt{2}}\left(|0\rangle + e^{i\pi x_1 + i\pi x_2/2}|1\rangle\right)$. Labeling the output state in the form of $|\Psi_{out}\rangle = |y_2\rangle \otimes |y_1\rangle$, the relative phase of the second qubit is twice that of the first qubit, which meets with the function of QFT.

As for the realization of quantum gates in the QFT circuit, the single-qubit H gate acting on either qubit has been discussed in Subsection 3.3. The two-qubit CS gate can be decomposed as $CS = CNOT \cdot (I \otimes T^{-1}) \cdot CNOT \cdot (T \otimes T)$ [see the equivalent circuit in Fig. 7(b)].[1] Similarly, the T^{-1} can be realized by inversing the sign of the gate voltage corresponding to the T quantum gate.

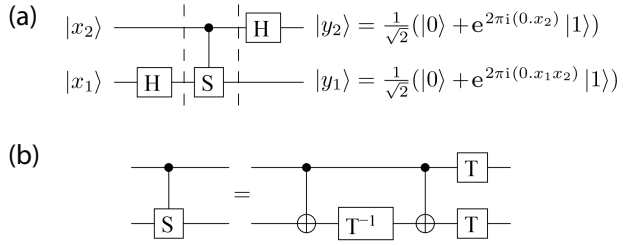


Fig. 7. (a) A two-qubit quantum circuit realizes the quantum Fourier transform. (b) The controlled-S gate is decomposed into the quantum gates CNOT and T. T^{-1} denotes the inverse of T gate, realizable by an opposite gate voltage of T gate.

Appealingly, the QFT algorithm with several quantum gates can be realized within the device shown Fig. 6(a). When the quantum state $|\Psi_{in}\rangle$ is initialized from three leads of the cells A1, A2, and A3, open the transfer boxes in the lowest row to convey the six chiral Majorana fermions to the cells B1, B2, and B3, and then close the transfer boxes. Tune the electric gates and quantum dots to apply the first H gate in cells B1 to B6 to produce the state $|\Psi_1\rangle$. Keep the transfer boxes in the highest row closed, so the state $|\Psi_1\rangle$ is carried back to the bottom of cells B1, B2, and B3, when the chiral Majorana fermions turn back and travel downward. Renew the electric gates and quantum dots of cells B1 to B6 to perform a new quantum gate. Repeat the above process until the last quantum gate is executed. Open the transfer boxes in the highest row to output the final state and finish the QFT computation. Based on the braiding of MZMs, the QFT algorithm is difficult to realize because the T quantum gate can not be realized. Here, the device in Fig. 6(a) based on chiral Majorana fermion can perform any two-qubit quantum algorithm under the control of the electric gate, the quantum-dot structure, and the transfer box.

5. Discussion on initialization and readout of qubits

Besides the quantum gates proposed above to realize quantum operations on qubits, here we briefly discuss the initialization and measurement of qubits based on chiral Majorana fermions.

Considering the conventional physical qubits, information is encoded in the degree of freedom such as photons, spin, or the electric charge. For the photon qubit,[3,6] the initialization is to create single photon states by attenuating laser light and drive them into certain polarization through optical polarizers and the measurement is to detect single photons, e.g., by

a photomultipler tube. For qubits realized by nuclear magnetic resonance,[79] the initial state is prepared in a strong magnetic field to polarize the spins and the readout process is to measure the voltage signal induced by precessing magnetic moment. As to the charge qubit based on the superconducting Josephson junctions[15] or the singly charged quantum dot pair,[10] the electron number is used as the basis state of qubit. These charge qubits can be initialized by electron injection via a current pulse or voltage pulse and the electronic charge state is straightforward to be measured by the quantum point contact or another quantum dots due to their high sensitivity to the conductance response to the applied gate voltage.[12,80,81]

Recalling our definition of qubit basis states [see the definition at the paragraph before Eq. (33)], four chiral Majorana fermions form a single qubit in the basis of ($|\mathbf{0}\rangle$, $|\mathbf{1}\rangle$), where $|\mathbf{0}\rangle$ stands for the left and right Dirac fermions being both empty and $|\mathbf{1}\rangle$ stands for those being both occupied. Since the encoded information via chiral Majorana femions is the electric charge, the initial state can be prepared by the electron injection via single-electron sources. With the recent decade development of the experimental technique of single-electron sources,[82] a single electron can be emitted by the AC single-electron source based on mesoscopic capacitor, pumped by dynamic semiconductor quantum dots, injected by voltage pulses, and so on. Levitov and collaborators predicted a special voltage pulse, a Lorentzian pulse, which injects an integer number of charge without other neutral excitation, named as a "leviton".[83–85] The Lorentzian pulse gives excellent control of electron numbers and has the advantage of injecting electrons at the Fermi energy with less decoherence from electron–hole relaxation processes. Dubois *et al.* experimentally demonstrated that Lorentzian pulses with integer charge give no noise except a weak thermal noise contribution so this kind of electron injection is suitable for charge qubits propagating in quantum conductors.[86]

Thus, our proposed qubit based on chiral Majorana fermions can be initialized when single-electron sources are connected to leads of the lower cells A1 and A2 [see the black squares labeled by 1 and 2 in Fig. 3(a)] to produce the basis state $|\mathbf{0}\rangle$ or $|\mathbf{1}\rangle$. Once the basis state is prepared, other quantum states are producible by applying the T gate and H gate, i.e., the initialization of qubit for further computation.

Based on our proposed qubit basis states ($|\mathbf{0}\rangle$ and $|\mathbf{1}\rangle$) being the empty and double occupied states, the readout way can be the single shot detection[87] or monitoring the charge by the quantum point contact at the upper cells C1 and C2 [see the black squares labeled by 3 and 4 in Fig. 3(a)].

Here it is worth mentioning that the partial exchange operation of the chiral Majorana fermions via these electric gates is not topologically protected. But it can be well controlled within the time scale ps, presenting the faster speed of information processing than physically moving or measuring Majorana zero modes. Except the gate operating region, the propagation of chiral Majorana fermions is topologically protected with no backscattering and no additional complex phase. Thus, our proposal owns the advantage of quantum computations based on chiral Majorana fermions: the fast speed of quantum computation well preserves and it partially displays the topological protection.

6. Conclusion

We have constructed the realization of arbitrary two-qubit quantum gates based on chiral Majorana fermions. The elementary cell which consists of a quantum anomalous Hall insulator surrounded by a topological superconductor with some electric gates and quantum-dot structures realizes the braiding operation and the partial exchange operation. Single-qubit operations, T and H quantum gates, are completed via one partial exchange and three braiding operations among four chiral Majorana fermions. An entangled two-qubit gate, the CNOT gate, is achieved via braiding six chiral Majorana fermions. We also show a design which can perform several quantum gate operations in series. These two-qubit quantum gates are used to the quantum circuit model of a simple quantum Fourier transform. This proposed device could be used for more interesting algorithm.

References

[1] Nielsen M A and Chuang I L 2010 *Quantum Computation and Quantum Information: 10th Anniversary Edition* (Cambridge: Cambridge University Press)
[2] Feynman R P 1982 *Int. J. Theor. Phys.* **21** 467
[3] Ladd T D, Jelezko F, Laflamme R, Nakamura Y, Monroe C and O'Brien J L 2010 *Nature* **464** 45
[4] Benioff P 1982 *J. Stat. Phys.* **29** 515
[5] DiVincenzo D P 1995 *Phys. Rev. A* **51** 1015
[6] Knill E, Laflamme R and Milburn G J 2001 *Nature* **409** 46
[7] Blatt R and Wineland D 2008 *Nature* **453** 1008
[8] Xu P, He X D, Liu M, Wang J and Zhan M S 2019 *Acta Phys. Sin.* **68** 030305 (in Chinese)
[9] Petta J R, Johnson A C, Taylor J M, Laird E A, Yacoby A, Lukin M D, Marcus C M, Hanson M P and Gossard A C 2005 *Science* **309** 2180
[10] Zhang X, Li H O, Wang K, Cao G, Xiao M and Guo G P 2018 *Chin. Phys. B* **27** 020305
[11] Wang K, Li H O, Xiao M, Cao G and Guo G P 2018 *Chin. Phys. B* **27** 090308
[12] Nakamura Y, Pashkin Y A and Tsai J S 1999 *Nature* **398** 786
[13] Chiorescu I, Nakamura Y, Harmans C J and Mooij J E 2003 *Science* **299** 1869
[14] Zhong Y P, Li C Y, Wang H H and Chen Y 2013 *Chin. Phys. B* **22** 110313
[15] Liu W Y, Zheng D N and Zhao S P 2018 *Chin. Phys. B* **27** 027401
[16] Nayak C, Simon S H, Stern A, Freedman M and Das Sarma S 2008 *Rev. Mod. Phys.* **80** 1083
[17] Sarma S D, Freedman M and Nayak C 2015 *npj Quantum Inf.* **1** 15001
[18] Elliott S R and Franz M 2015 *Rev. Mod. Phys.* **87** 137
[19] Bravyi S 2006 *Phys. Rev. A* **73** 042313
[20] Kitaev A Y 2003 *Ann. Phys.* **303** 2
[21] Ivanov D A 2001 *Phys. Rev. Lett.* **86** 268
[22] Beenakker C W J 2013 *Annu. Rev. Condens. Matter Phys.* **4** 113
[23] Alicea J 2012 *Rep. Prog. Phys.* **75** 076501
[24] Kitaev A Y 2001 *Phys.-Usp.* **44** 131
[25] Qi J J, Liu H W, Jiang H and Xie X C 2019 *Front. Phys.* **14** 43403

[26] Li Y H, Liu J, Song J T, Jiang H, Sun Q F and Xie X C 2018 *Sci. China Phys. Mech. Astron.* **61** 97411
[27] Chen C Z, Jiang H, Xu D H and Xie X C 2020 *Sci. China Phys. Mech. Astron.* **63** 107811
[28] Yang Y T, Jia Z Y, Wu Y J, Xiao R C, Hang Z H, Jiang H and Xie X C 2020 *Sci. Bull.* **65** 531
[29] Fu L and Kane C L 2008 *Phys. Rev. Lett.* **100** 096407
[30] Fu L and Kane C L 2009 *Phys. Rev. B* **79** 161408(R)
[31] Lutchyn R M, Sau J D and Das Sarma S 2010 *Phys. Rev. Lett.* **105** 077001
[32] Oreg Y, Refael G and von Oppen F 2010 *Phys. Rev. Lett.* **105** 177002
[33] Zheng H and Jia J F 2019 *Chin. Phys. B* **28** 067403
[34] Liu J, Wu Y, Sun Q F and Xie X C 2019 *Phys. Rev. B* **100** 235131
[35] Sau J D, Lutchyn R M, Tewari S and Das Sarma S 2010 *Phys. Rev. Lett.* **104** 040502
[36] Tang H Z, Sun Q F, Liu J J and Zhang Y T 2019 *Phys. Rev. B* **99** 235427
[37] Law K T, Lee P A and Ng T K 2009 *Phys. Rev. Lett.* **103** 237001
[38] Mourik V, Zuo K, Frolov S M, Plissard S, Bakkers E P and Kouwenhoven L P 2012 *Science* **336** 1003
[39] Nadj-Perge S, Drozdov I K, Li J, Chen H, Jeon S, Seo J, MacDonald A H, Bernevig B A and Yazdani A 2014 *Science* **346** 602
[40] Zhang P, Yaji K, Hashimoto T, Ota Y, Kondo T, Okazaki K, Wang Z J, Wen J S, Gu G D, Ding H and Shin S 2018 *Science* **360** 182
[41] Jäck B, Xie Y L, Li J, Jeon S, Bernevig B A and Yazdani A 2019 *Science* **364** 1255
[42] Laroche D, Bouman D, van Woerkom D J, Proutski A, Murthy C, Pikulin D I, Nayak C, van Gulik R J J, Nygard J, Krogstrup P, Kouwenhoven L P and Geresdi A 2019 *Nat. Commun.* **10** 245
[43] Alicea J, Oreg Y, Refael G, von Oppen F and Fisher M P 2011 *Nat. Phys.* **7** 412
[44] Halperin B I, Oreg Y, Stern A, Refael G, Alicea J and von Oppen F 2012 *Phys. Rev. B* **85** 144501
[45] Bonderson P, Freedman M and Nayak C 2008 *Phys. Rev. Lett.* **101** 010501
[46] Bonderson P, Freedman M and Nayak C 2009 *Ann. Phys.* **324** 787
[47] Fu L 2010 *Phys. Rev. Lett.* **104** 056402
[48] Vijay S and Fu L 2016 *Phys. Rev. B* **94** 235446
[49] Karzig T, Knapp C, Lutchyn R M, Bonderson P, Hastings M B, Nayak C, Alicea J, Flensberg K, Plugge S, Oreg Y, Marcus C M and Freedman M H 2017 *Phys. Rev. B* **95** 235305
[50] Campbell E T, Terhal B M and Vuillot C 2017 *Nature* **549** 172
[51] Fowler A G, Mariantoni M, Martinis J M and Cleland A N 2012 *Phys. Rev. A* **86** 032324
[52] Wang J 2020 *Acta Phys. Sin.* **69** 117302 (in Chinese)
[53] Chang C Z, Zhang J, Feng X, Shen J, Zhang Z, Guo M, Li K, Ou Y, Wei P, Wang L L, Ji Z Q, Feng Y, Ji S, Chen X, Jia J, Dai X, Fang Z, Zhang S C, He K, Wang Y, Lu L, Ma X C and Xue Q K 2013 *Science* **340** 167
[54] He K, Ma X C, Chen X, Lu L, Wang Y Y and Xue Q K 2013 *Chin. Phys. B* **22** 067305
[55] He K 2020 *Physics* **49** 828
[56] Fu L and Kane C L 2009 *Phys. Rev. Lett.* **102** 216403
[57] Akhmerov A R, Nilsson J and Beenakker C W J 2009 *Phys. Rev. Lett.* **102** 216404
[58] Qi X L, Hughes T L and Zhang S C 2010 *Phys. Rev. B* **82** 184516
[59] Zhang J, Zhao B, Zhou T and Yang Z 2016 *Chin. Phys. B* **25** 117308
[60] Wang J, Zhou Q, Lian B and Zhang S C 2015 *Phys. Rev. B* **92** 064520
[61] Yan Q, Zhou Y F and Sun Q F 2020 *Chin. Phys. B* **29** 097401
[62] Zhang Y T, Hou Z, Xie X C and Sun Q F 2017 *Phys. Rev. B* **95** 245433
[63] Zhou Y F, Hou Z, Zhang Y T and Sun Q F 2018 *Phys. Rev. B* **97** 115452
[64] Yan Q, Zhou Y F and Sun Q F 2019 *Phys. Rev. B* **100** 235407
[65] Zhou Y F, Hou Z, Lv P, Xie X and Sun Q F 2018 *Sci. China Phys. Mech. Astron.* **61** 127811
[66] He Q L, Pan L, Stern A L, Burks E C, Che X, Yin G, Wang J, Lian B, Zhou Q, Choi E S, Murata K, Kou X, Chen Z, Nie T, Shao Q, Fan Y, Zhang S C, Liu K, Xia J and Wang K L 2017 *Science* **357** 294
[67] Huang Y, Setiawan F and Sau J D 2018 *Phys. Rev. B* **97** 100501(R)
[68] Ji W and Wen X G 2018 *Phys. Rev. Lett.* **120** 107002
[69] Chen C Z, He J J, Xu D H and Law K T 2017 *Phys. Rev. B* **96** 041118
[70] Lian B, Wang J, Sun X Q, Vaezi A and Zhang S C 2018 *Phys. Rev. B* **97** 125408
[71] Kayyalha M, Xiao D, Zhang R X, Shin J, Jiang J, Wang F, Zhao Y F, Xiao R, Zhang L, Fijalkowski K M, Mandal P, Winnerlein M, Gould C, Li Q, Molenkamp L W, Chan M H W, Samarth N and Chang C Z 2020 *Science* **367** 64
[72] Lian B, Sun X Q, Vaezi A, Qi X L and Zhang S C 2018 *Proc. Natl. Acad. Sci. USA* **115** 10938
[73] Zhou Y F, Hou Z and Sun Q F 2019 *Phys. Rev. B* **99** 195137
[74] Beenakker C W J, Baireuther P, Herasymenko Y, Adagideli I, Wang L and Akhmerov A R 2019 *Phys. Rev. Lett.* **122** 146803
[75] Zwanenburg F A, Dzurak A S, Morello A, Simmons M Y, Hollenberg L C L, Klimeck G, Rogge S, Coppersmith S N and Eriksson M A 2013 *Rev. Mod. Phys.* **85** 961
[76] Georgiev L S 2006 *Phys. Rev. B* **74** 235112
[77] Kaye P, Laflamme R and Mosca M 2007 *An introduction to quantum computing* (Oxford: Oxford University Press)
[78] Beenakker C W J 2020 *SciPostPhys. Lect. Notes* **15**
[79] Kong X Y, Zhu Y Y, Wen J W, Xin T, Li K R and Long G L 2018 *Acta Phys. Sin.* **67** 220301 (in Chinese)
[80] Su F F, Wang Z T, Xu H K, Zhao S K, Yan H S, Yang Z H, Tian Y and Zhao S P 2019 *Chin. Phys. B* **28** 110303
[81] Yan L, Yin W and Wang F W 2014 *Chin. Phys. B* **23** 100303
[82] Bäuerle C, Glattli D C, Meunier T, Portier F, Roche P, Roulleau P, Takada S and Waintal X 2018 *Rep. Prog. Phys.* **81** 056503
[83] Levitov L S, Lee H and Lesovik G B 1996 *J. Math. Phys.* **37** 4845
[84] Ivanov D A, Lee H W and Levitov L S 1997 *Phys. Rev. B* **56** 6839
[85] Keeling J, Klich I and Levitov L S 2006 *Phys. Rev. Lett.* **97** 116403
[86] Dubois J, Jullien T, Portier F, Roche P, Cavanna A, Jin Y, Wegscheider W, Roulleau P and Glattli D C 2013 *Nature* **502** 659
[87] Bocquillon E, Freulon V, Berroir J M, Degiovanni P, Plaçais B, Cavanna A, Jin Y and Fève G 2013 *Science* **339** 1054